# Adaptive Droop Control Applied to Voltage-Source Inverters Operating in Grid-Connected and Islanded Modes

Juan C. Vasquez, Josep M. Guerrero, *Senior Member, IEEE*, Alvaro Luna,
Pedro Rodríguez, *Member, IEEE*, and Remus Teodorescu, *Senior Member, IEEE*

*Abstract*—**This paper proposes a novel control for voltage-source inverters with the capability to flexibly operate in grid-connected and islanded modes. The control scheme is based on the droop method, which uses some estimated grid parameters such as the voltage and frequency and the magnitude and angle of the grid impedance. Hence, the inverter is able to inject independently active and reactive power to the grid. The controller provides a proper dynamics decoupled from the grid-impedance magnitude and phase. The system is also able to control active and reactive power flows independently for a large range of impedance grid values. Simulation and experimental results are provided in order to show the feasibility of the control proposed.**

*Index Terms*—**DC–AC power conversion, distributed generation (DG), droop control, impedance estimation, power generation control, voltage-source inverters (VSIs).**

## I. INTRODUCTION

**D**ISTRIBUTED generation (DG) systems and microgrids are becoming more and more important when trying to increase the renewable energy penetration. In this sense, the use of intelligent power interfaces between the electrical generation sources and the grid is mandatory. These interfaces have a final stage consisting of dc/ac inverters, which can be classified in current-source inverters (CSIs) and voltage-source inverters (VSIs). In order to inject current to the grid, CSIs are commonly used, while in island or autonomous operation, VSIs are needed to keep the voltage stable [1].

VSIs are very interesting for DG applications since they do not need any external reference to stay synchronized [2], [3]. In fact, they can operate in parallel with other inverters by using frequency and voltage droops, forming autonomous or isolated microgrids [4]. Furthermore, VSIs are convenient since they can provide to distributed power generation systems performances like ride-through capability and power quality enhance-

ment [5], [6], [25]–[31]. When these inverters are required to operate in grid-connected mode, they often change its behavior from voltage to current sources [7]. Nevertheless, to achieve flexible microgrids, i.e., able to operate in both grid-connected and islanded modes, VSIs are required to control the exported or imported power to the mains grid and to stabilize the microgrid [8], [9]. In this sense, the droop method can be used to inject active and reactive power from the VSI to the grid by adjusting the frequency and amplitude of the output voltage [2]–[4]. However, the conventional droop method needs the knowledge of some parameters of the grid in order to control independently the active and reactive power flows. In this sense, the estimation of the grid impedance can be interesting not only for injecting $P$ and $Q$ into the grid with high precision but also for islanding detection.

In this paper, we propose a control scheme based on the droop method which automatically adjusts their parameters by using a grid-impedance estimation method based on analyzing the voltage and current variations at the point of common coupling (PCC) resulting from small deviations in the power generated by the VSI [11]. The VSI is able to operate in both grid-connected and islanded modes, as well as to seamlessly transfer between these modes. This paper is organized as follows. In Section II, the grid parameters are obtained by using an estimation algorithm. With these estimated parameters, an adaptive droop-control method is presented in Section III, which is able to decouple active and reactive power flow. Simulation results are presented in Section V to illustrate the feasibility of the proposed controller. Section VI shows the experimental results. Finally, Section VII gives the conclusion.

## II. ESTIMATION OF THE GRID PARAMETERS

The grid characterization technique used in this paper is based on processing the voltage and current phasors at the PCC between the power converter and the grid. A frequency-locked loop based on the second-order generalized integrator (SOGI-FLL) is used to monitor such voltage and current phasors. As shown in Fig. 1, two cascaded integrators working in closed loop are used to implement the SOGI [10], [11]. This grid monitoring technique provides high precision, low computational cost, and frequency adaptation capability [11], [24].

The aforementioned SOGI-FLL is also applied to monitor the current injected into the PCC in order to obtain the current phasor $\vec{I} = i_d + ji_q$. The SOGI-FLL acts as a selective filter
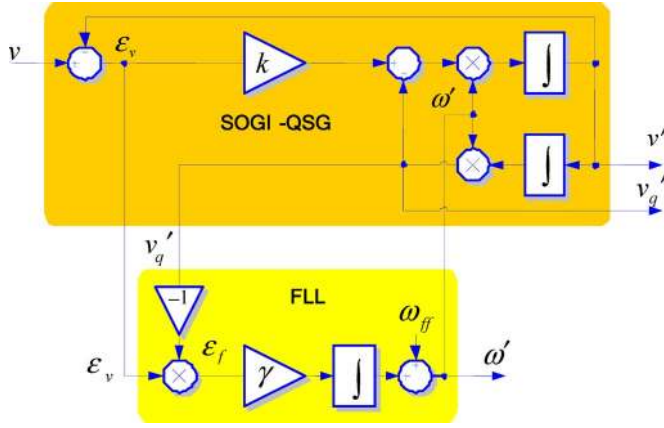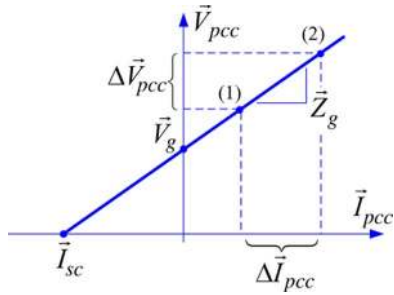
Fig. 1. Diagram of the SOGI-FLL.



Fig. 2. *V*–*I* characteristic of the grid for a particular frequency.

for detecting two in-quadrature output signals, which is a very interesting feature to attenuate harmonics on the monitored voltage and current and accurately detect the phasors of the grid voltage and current ($\vec{V}_g$ and $\vec{I}_g$) at the fundamental grid frequency. The detected voltage and current in-quadrature signals are projected on a $d$–$q$ rotating reference frame to obtain coherent voltage and current phasors.

The technique used for estimating the grid parameters stems from a linear interpretation of the grid in which distributed power generators are connected to. Therefore, the grid can be seen from the PCC of a power generator as a simple Thevenin circuit—constituted by a grid impedance $\vec{Z}_g$ and a header voltage $\vec{V}_g$. Even though the $V$–$I$ characteristic of the ac grid cannot be represented by a simple 2-D Cartesian plane, Figs. 2 and 3 help to show further explanations about the impedance detection method used in this paper since it depicts the relationship between voltage and current phasors at the PCC for a particular frequency.

From the measurement of the voltage and current phasors at the PCC at two different operating points, the linearity in the $V$–$I$ characteristic of Fig. 2 allows for writing (1) and (2) and for estimating the grid impedance $\vec{Z}_g$ and the open-circuit voltage $\vec{V}_g$, respectively

$$\vec{Z}_g = Z_g \angle \theta_g = \frac{\Delta \vec{V}_{\text{pcc}}}{\Delta \vec{I}_{\text{pcc}}} = \frac{\vec{V}_1 - \vec{V}_2}{\vec{I}_1 - \vec{I}_2} \quad (1)$$

$$\vec{V}_g = V_g \angle \phi_g = \vec{V}_{\text{pcc}(i)} - \vec{Z}_g \vec{I}_{\text{pcc}(i)} = \frac{\vec{I}_1 \vec{V}_2 - \vec{I}_2 \vec{V}_1}{\vec{I}_1 - \vec{I}_2} \quad (2)$$
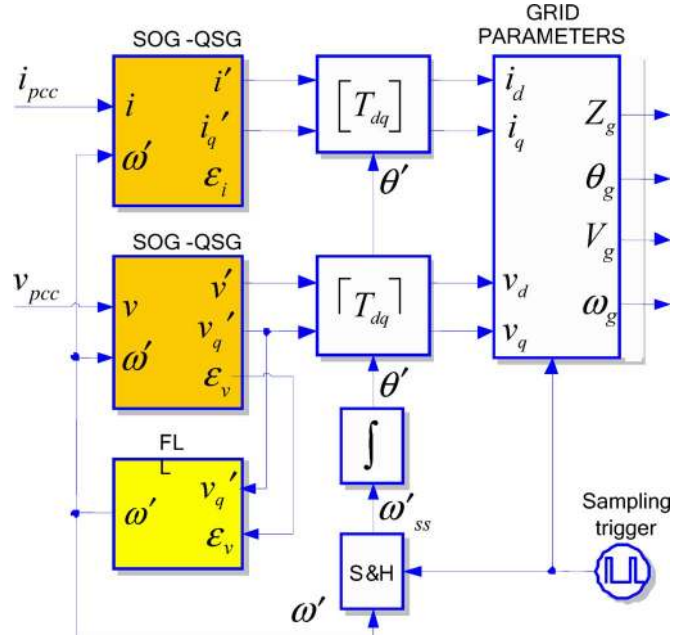


Fig. 3. Block diagram of the grid parameter identification algorithm.

where $Z_g$ and $\theta_g$ are the magnitude and the angle grid impedance, respectively. Several techniques for detecting the grid impedance are either directly or indirectly based on this basic principle [14]–[18]. In this paper, the grid parameters are estimated from the active and reactive power variations generated by a grid-connected converter in which a droop controller is implemented. The cornerstone of this estimation technique is the accuracy in the online measurement of voltage and current phasors at the PCC, which is performed based on the SOGI-FLL. Fig. 3 shows the diagram of the algorithm used in this paper to identify the grid parameters. It is worthy to say that the estimated values of the angle and magnitude of the grid voltage impedance and their voltage and frequency are transiently wrong after each change in the grid parameters. Therefore, as shown in Fig. 3, the FLL block is only implemented on the monitored voltage $v$, and the angle $\theta'$ is calculated from the integration of the voltage frequency.

As transient values cannot be sent to the droop controller of the VSI, a small buffer of three rows is added at the output of the grid parameter identification block of Fig. 3.

## III. ADAPTIVE DROOP CONTROL

In this section, based on the estimation of the grid parameters provided by the identification algorithm, an adaptive droop controller that is able to inject active and reactive power into the grid with high accuracy is proposed.

### A. Power Flow Analysis

From Fig. 4, we can calculate the active and reactive powers injected to the grid by the VSI [19], [20]

$$P = \frac{1}{Z_g} \left[ \left( EV_g \cos\phi - V_g^2 \right) \cos\theta_g + EV_g \sin\phi \sin\theta_g \right] \quad (3a)$$

$$Q = \frac{1}{Z_g} \left[ \left( EV_g \cos\phi - V_g^2 \right) \sin\theta_g - EV_g \sin\phi \cos\theta_g \right] \quad (3b)$$
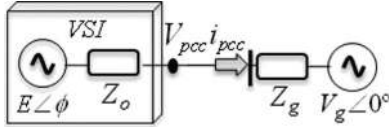
Fig. 4.   Equivalent circuit of the VSI connected to the grid.

where $E$ and $\phi$ are the magnitude and phase of the VSI, respectively, and $V_g$ is the grid voltage. Notice that both expressions depend highly on the grid impedance ($Z_g \angle \theta_g$). Consequently, we propose to transform $P$ and $Q$ into novel variables ($P_c$ and $Q_c$) which are independent from the magnitude and phase of the grid impedance

$$P_c = Z_g(P \sin \theta_g - Q \cos \theta_g) \tag{4a}$$
$$Q_c = Z_g(P \cos \theta_g + Q \sin \theta_g). \tag{4b}$$

By substituting (3) into (4), it yields the following:

$$P_c = EV_g \sin \phi \tag{5a}$$
$$Q_c = EV_g \cos \phi - V_g^2. \tag{5b}$$

Note that $P_c$ is mainly dependent on the phase $\phi$, while $Q_c$ depends on the voltage difference between the VSI and the grid ($E - V_g$).

Once these control variables ($P_c$ and $Q_c$) are obtained, we can use them into the droop-control method to inject active and reactive power.

## B. Droop-Control Technique

With the aim to inject the desired active and reactive powers (defined as $P^*$ and $Q^*$), the following droop-control method which uses the transformation (4) is proposed:

$$\phi = -G_p(s)Z_g[(P-P^*)\sin\theta_g - (Q-Q^*)\cos\theta_g] \tag{6a}$$
$$E = E^* - G_q(s)Z_g[(P-P^*)\cos\theta_g + (Q-Q^*)\sin\theta_g] \tag{6b}$$

where $E^*$ is the amplitude voltage reference, which takes the values of the estimated grid voltage ($V_g$). By using these equations, we can obtain the voltage reference of the VSI $v_{\text{ref}}^* = E \sin(\omega^* t + \phi)$, where $\omega^*$ is the frequency reference.

The compensator transfer functions of $P_c$ and $Q_c$ can be expressed as

$$G_p(s) = \frac{m_i + m_p s + m_d s^2}{s} \tag{7a}$$
$$G_q(s) = \frac{n_i + n_p s}{s}. \tag{7b}$$

Note that, in practice, the derivative term in $G_q(s)$ is avoided since it barely affects the system dynamics.

Fig. 5 shows the block diagram of the droop controller proposed to inject the desired active $P^*$ and reactive power $Q^*$.

## C. System Dynamics

In order to show the system stability and the transient response, a small-signal analysis is provided, allowing the designer to adjust the control parameters [21], [22]. Taking into
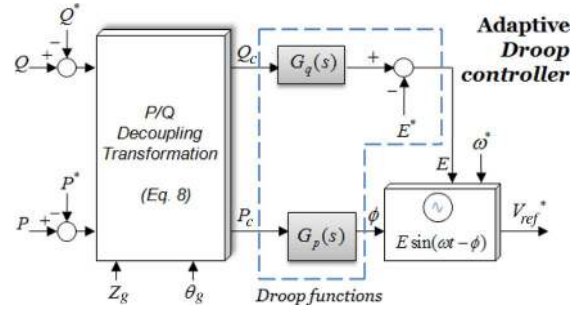


Fig. 5.   Block diagram of the adaptive droop control.

account that $P$ and $Q$ are the average values of instantaneous active and reactive power $p(t)$ and $q(t)$

$$P = \overline{v_d i_d} + \overline{v_q i_q} = \frac{1}{T} \int_t^{t-T} p(t)dt \tag{8a}$$

$$Q = \overline{v_q i_d} - \overline{v_d i_q} = \frac{1}{T} \int_t^{t-T} q(t)dt \tag{8b}$$

where $T$ is the period of the grid frequency. By using the first-order Padé approximation

$$e^{-Ts} \approx \frac{2 - Ts}{2 + Ts} \tag{9}$$

the average value $P$ and $Q$ can be expressed as follows:

$$P = \frac{1 - e^{-Ts}}{Ts}p(s) \approx \frac{1}{1 + (T/2)s}p(s) \tag{10a}$$

$$Q = \frac{1 - e^{-Ts}}{Ts}q(s) \approx \frac{1}{1 + (T/2)s}q(s). \tag{10b}$$

By substituting (9) and (10) into (14) and using the small signal approximation to linearize the equations, we yield

$$\hat{p}_c(s) = \frac{1}{1 + t(T/2)s}\left(V_g \sin\Phi\hat{e}(s) + V_g E \cos\Phi\hat{\phi}(s)\right) \tag{11a}$$

$$\hat{q}_c(s) = \frac{1}{1 + (T/2)s}\left(V_g \cos\Phi\hat{e}(s) - V_g E \sin\Phi\hat{\phi}(s)\right) \tag{11b}$$

where the lowercase variables with the symbol ^ indicate small-signal values and the uppercase variables are the steady-state values. By using (6), (7), and (11), the following can be obtained:

$$\hat{\phi}(s) = -\left(\frac{m_i + m_p s + m_d s^2}{s}\right)\hat{p}_c(s) \tag{12a}$$

$$\hat{e}(s) = -\left(\frac{n_i + n_p s}{s}\right)\hat{q}_c(s). \tag{12b}$$

From (12), the following can be derived:

$$\hat{\phi}(s) = -\left(\frac{m_i + m_p s + m_d s^2}{s}\right)\frac{V_g \sin\Theta\hat{e}(s) + V_g E \cos\Theta\hat{\phi}(s)}{1 + (T/2)s} \tag{13a}$$

$$\hat{e}(s) = -\left(\frac{n_i + n_p s}{s}\right)\frac{V_g \cos\Theta\hat{e}(s) + V_g E \sin\Theta\hat{\phi}(s)}{1 + (T/2)s}. \tag{13b}$$
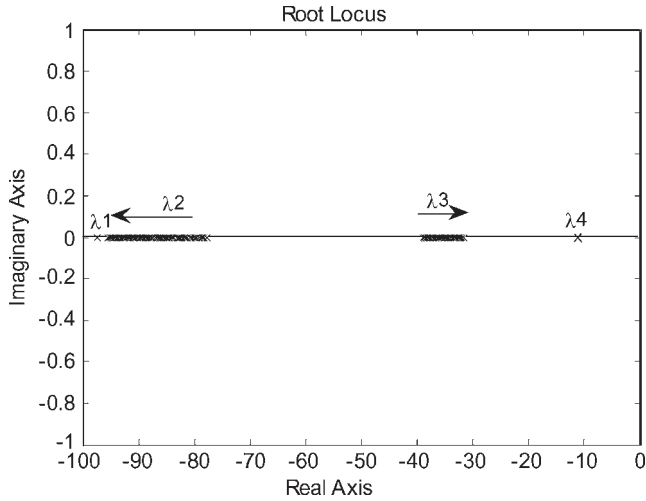
Fig. 6.  Trace of root locus for $0.00005 < m_p < 0.0001$.



Fig. 7.  Trace of root locus for $1 \times 10^{-6} < m_d < 4 \times 10^{-5}$.

By combining (13a) and (13b), the following fourth-order characteristic equation can be obtained:

$$a_4 s^4 + a_3 s^3 + a_2 s^2 + a_1 s + a_0 = 0 \qquad (14)$$

where

$$
\begin{aligned}
a_4 &= T^2 + 2T m_d V_g E \cos \Phi \\
a_3 &= 4T + 4 m_d n_p V_g^2 E + 2 V_g \cos \Phi \\
&\quad \times (2 m_d E + T n_p + T m_p E) \\
a_2 &= 2 V_g \cos \Phi (T m_i E + T n_i + 2 n_p + 2 m_p) \\
&\quad + 4 V_g^2 E (m_p n_p + m_d n_i) + 4 \\
a_1 &= 4V \cos \Phi (n_i + m_i E) + 4 V^2 E (m_i n_p + m_p n_i) \\
a_0 &= 4 n_i m_i E V^2
\end{aligned}
$$

where the steady-state values of the active and reactive power are $P = P^*$ and $Q = Q^*$, and from (3), the steady-state phase and amplitudes can be calculated as follows:

$$\Phi = \tan^{-1} \left( \frac{P^* \sin \theta_g - Q^* \cos \theta_g}{P^* \cos \theta_g + Q^* \sin \theta_g + (V_g^2 / Z_g)} \right) \qquad (15a)$$

$$E = \frac{V_g^2 \cos \theta_g + P^* Z_g}{V_g (\cos \theta_g \cos \Phi + \sin \theta_g \sin \Phi)}. \qquad (16b)$$

By using this model, we can extract the root locus family that is shown in Figs. 6–8 by changing $m_p$, $m_d$, and $n_d$. In order to guarantee the stability condition (input/output behavior) of the closed-loop system dynamics, a pole study of the fourth-order identified model is employed. The performance of this kind of systems is often viewed in terms of pole dominance. The $a_0$ coefficient of the characteristic equation depends basically on the $m_i$ and $n_i$ parameters that influence directly over the system fast response, making it more damped. In some practical cases, it is possible to adjust these parameters for fine-tuning purposes.

Moreover, system stability can be determined by using (14) when the islanding mode is taking place. In an autonomous operation mode, the system stability can be compromised if any reactive power contributions from the main grid are considered. It is possible to solve if the parameter $n_i$ in (14) equals zero,
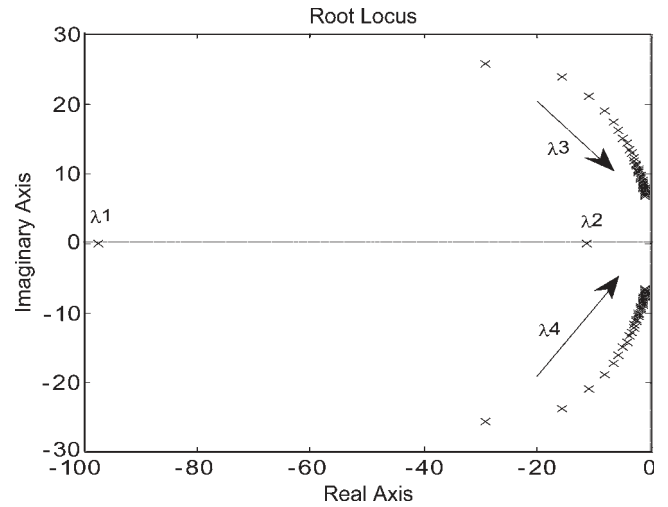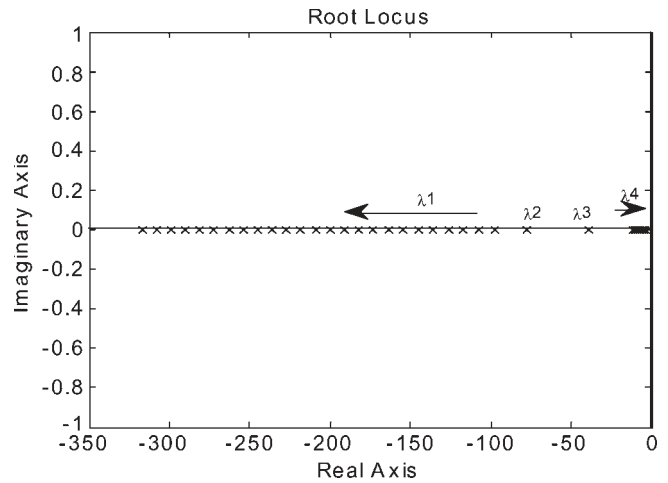


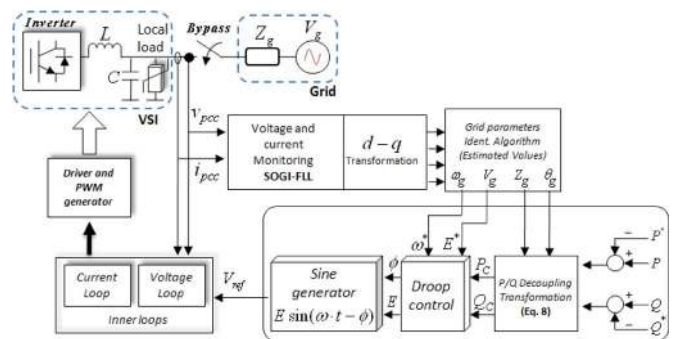Fig. 8.  Trace of root locus for $0.0004 < n_p < 0.01$.



Fig. 9.  Block diagram of the SOGI and proposed adaptive droop control with grid-connected to autonomous mode transition capability.

reducing the system dynamics to a third-order equation. That is why the fourth-order system can be simplified to a third-, second-, or even first-order system.

## IV. CONTROL STRUCTURE

Fig. 9 shows the proposed block diagram of the whole control structure of the VSI unit. It consists of several control loops, described as follows. The inner control loops regulate
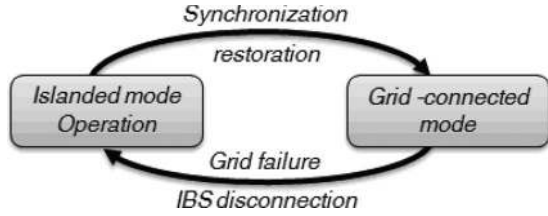
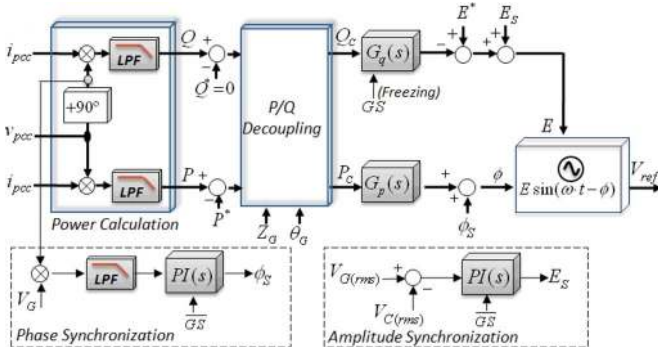Fig. 10. Flowchart diagram of the modes of the VSI.



Fig. 11. Block diagram of the whole proposed controller using the synchronization control loops.

TABLE I
SYSTEM PARAMETERS

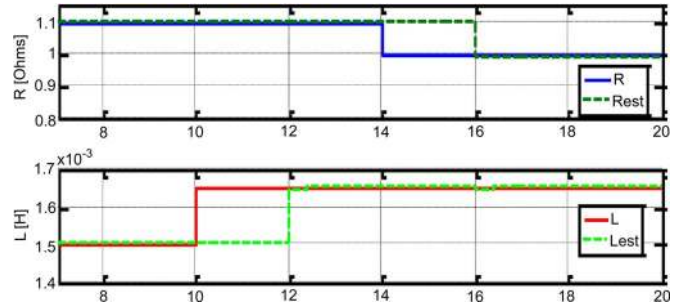| Parameter | Symbol | Value | Units |
|---|---|---|---|
| Voltage grid | $V_g$ | 311 | V |
| Frequency grid | $\omega^*$ | 50 | Hz |
| Resistive part of $Z_g$ | $R_g$ | 2 | $\Omega$ |
| Indutive part of $Z_g$ | $L_g$ | 3 | mH |
| Grid impedance module | $Z_g$ | 2.3 | $\Omega$ |
| Grid impedance angle | $\theta_g$ | 28.8 | deg |
| Integral phase droop | $m_i$ | 0.0018 | Ws/rd |
| Proportional phase droop | $m_p$ | 0.00005 | W/rd |
| Derivative phase droop | $m_d$ | $7 \cdot 10^{-7}$ | W/rd·s |
| Integral amplitude droop | $n_i$ | 0.15 | VAr·s/V |
| Derivative amplitude droop | $n_p$ | 0.0004 | VAr/V |



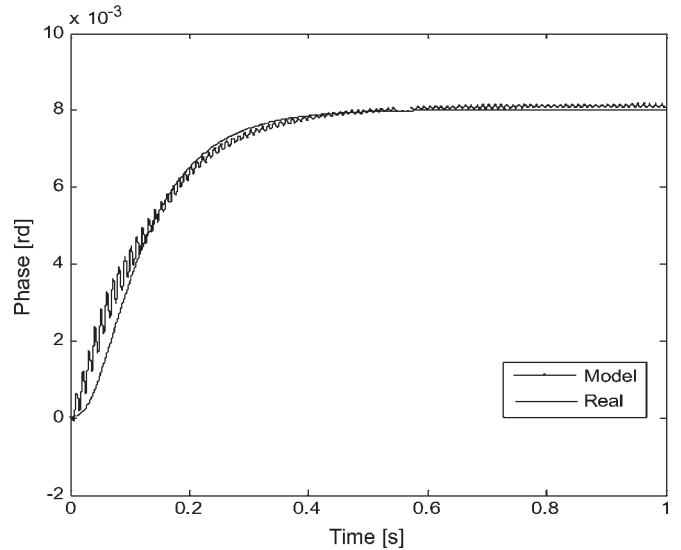Fig. 12. Variations of the grid impedance $R$ and $L$ estimation.



Fig. 13. Dynamic response of the system and the model (14).

the inverter output voltage and limit the output current. The loop of the SOGI-FLL and the associated algorithm is able to estimate the grid parameters: the frequency, voltage, and magnitude and angle of the grid impedance ($\omega_g$, $V_g$, $Z_g$, and $\theta_g$). These parameters are used by the adaptive droop controller to inject the required active and reactive power by the VSI into the grid. In addition, the estimation of the grid impedance can be useful for islanding detection. If $Z_g < 1.75$ $\Omega$ or $Z_g$ changes more than 0.5 $\Omega$ in 5 s, the VSI will be in island mode. Islanding detection is necessary in order to achieve a soft transition between grid-connected and islanding modes for a nonplanned islanding scenario. In that case, the integral term of the reactive power control must be disconnected ($n_i = 0$) [23].

Fig. 10 shows the flowchart diagram of the two operation modes of the inverter and their transitions. Starting from the islanding mode, the VSI is supplying the local load. When the grid is available, the VSI must start the synchronization process with the phase, frequency, and amplitude of the grid, without connecting the bypass switch (indicated by the grid status variable /$GS$ in Fig. 11). The phase and frequency synchronization can be done by multiplying the quadrature component of the voltage grid by the VSI voltage and processing this signal through a low-pass filter and a PI controller to be sent to the phase control loop, as shown in Fig. 11. In order to adjust the voltage amplitude, the *rms* voltage error between the grid and the VSI must be calculated and processed through a PI to be sent to the amplitude control loop. Hence, after several line cycles, the VSI will be synchronized to the grid, and the bypass can interconnect the VSI and the grid. At this moment, the desired active and reactive powers can be injected to the grid.

## V. SIMULATION RESULTS

The proposed control is tested through proper simulations in order to validate its feasibility. A single-phase VSI with the controller proposed was simulated by using the control and system parameters shown in Table I.

Fig. 12 shows the grid-impedance estimator performance. The inductive part of the grid impedance changes from 1.50 to 1.65 mH at $t = 10$ s, while the resistive part changes from 1.1 to 1 $\Omega$ at $t = 14$ s. As can be observed, the transient values cannot be sent directly to the droop controller of the VSI. For that reason, a small mismatch is appreciated due to the buffer of the grid parameter estimation algorithm (see Section II).

Fig. 13 shows the validity of the model, showing the good resemblance between the system phase dynamics and the obtained model (14). The model has been proved for a wide range of grid-impedance values, showing its validity.
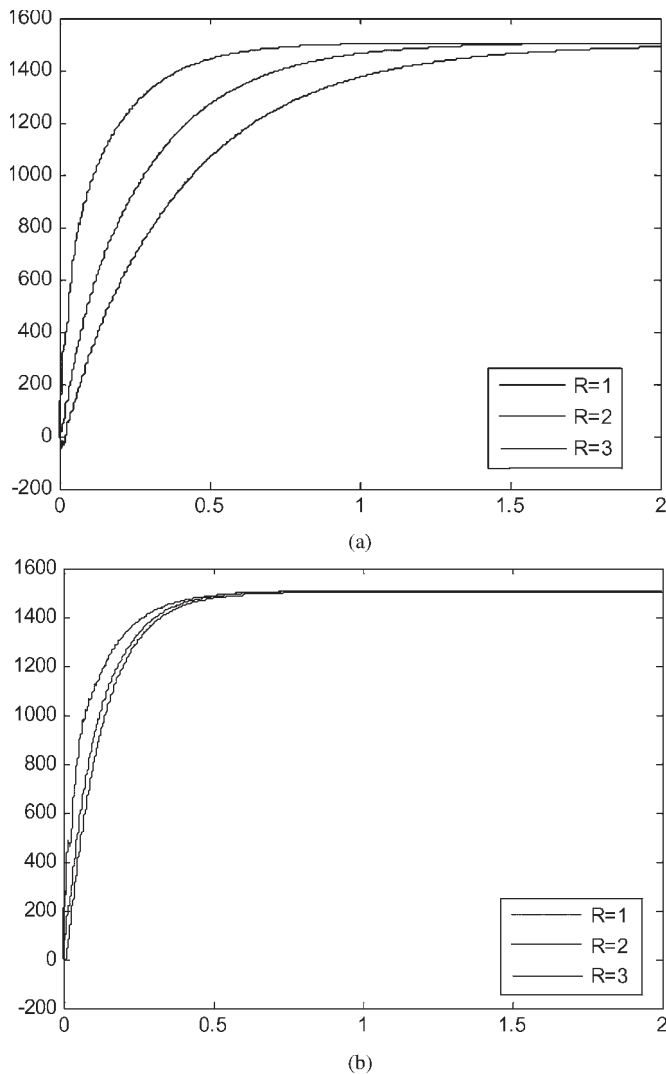
Fig. 14. Start-up of $P$ for different line impedances (a) without and (b) with the estimation algorithm of $Z_g$.
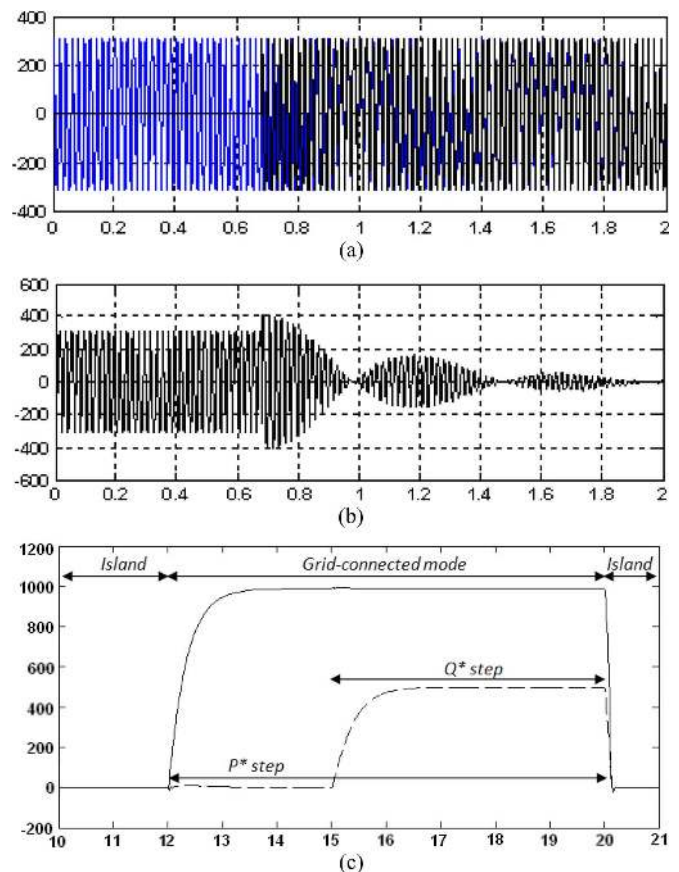


Fig. 15. Transition from islanding to grid-connected mode. (a) Synchronization process (grid and VSI voltages). (b) Error between grid and inverter voltages. (c) $P$ and $Q$ for $t < 12$ s in islanding mode and $t > 12$ s in grid-connected mode. In $t = 17$ s, $P$ changes from 0 to 1000 W, in $t = 19$ s, $Q$ changes from 0 to 500 var, and in $t = 20$ s, the system is disconnected from the grid.

In addition, to illustrate the robustness in front of large grid-impedance variations, some simulations have been performed with and without the estimator algorithm. Fig. 14 shows the transient response of the active power by using the control without and with the grid-impedance estimation loop, for grid-impedance variations $(R_g = 1, 2,$ and $3\ \Omega)$. Notice that this loop decouples, to a large extent, the system dynamics from the grid-impedance value.

Fig. 15(a) shows the synchronization process of the output voltage inverter with respect to the grid voltage, during islanding operation. Fig. 15(b) shows the voltage difference between the voltage grid and VSI voltages. Once the synchronization is done, Fig. 15(c) shows the transition from islanded to grid-connected mode. When the connection is realized and the system is under steady-state condition, the active and reactive power injected to the grid can be independently controlled. Finally, the system is intentionally disconnected $(t = 20$ s) in order to validate the transition operation from grid-connected to islanded mode. The seamless transfer between both modes can be seen, pointing out the flexible operation of the VSI.
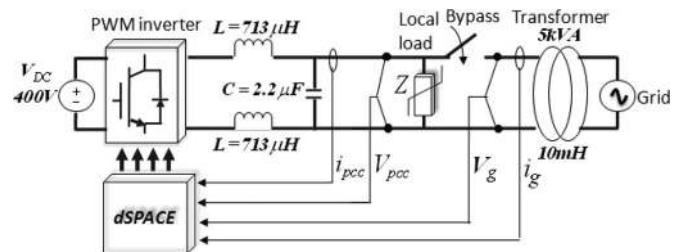


Fig. 16. Scheme of the experimental setup.

## VI. EXPERIMENTAL RESULTS

Experiments have been performed in order to show the feasibility of the controller proposed. The hardware setup shown in Fig. 16 consists of the following equipment: a Danfoss VLT 5006 7.6-kVA inverter with an $LC$ filter $(L = 2 \times 712\ \mu H$ and $C = 2.2\ \mu F)$ and a local load. A dSPACE 1104 system is used to implement the controller. The system sampling and switching frequency were running at 8 kHz.

The inverter is connected, through a bypass switch, to a 5-kVA low-voltage grid transformer with an equivalent impedance of 10 mH. The waveforms presented here were obtained through the ControlDesk software provided by dSPACE, as shown in Fig. 17.
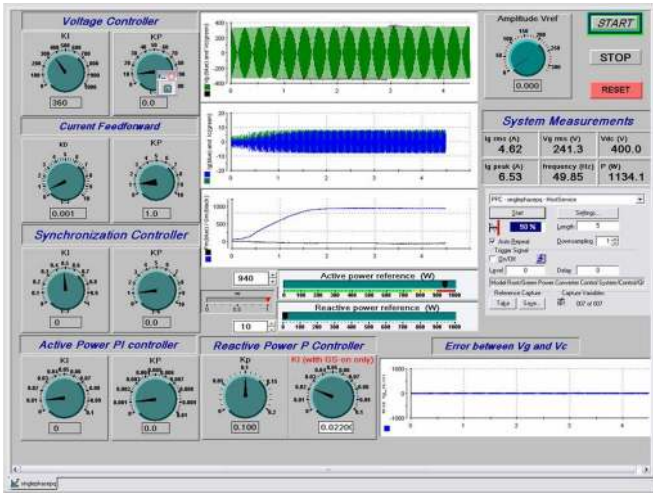
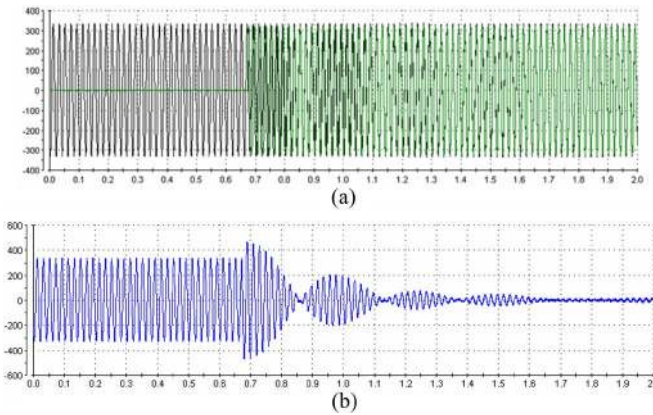Fig. 17. Panel supervisor of the ControlDesk from dSPACE.



Fig. 18. Synchronization of the inverter to the grid. (a) Grid and inverter voltage waveforms. (b) Error between grid and inverter voltages.
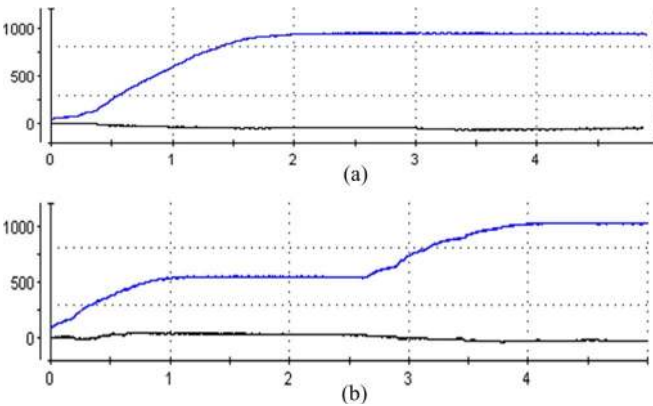


Fig. 19. Active power transient response for $Q = 0$ var. (a) From 0 to 1000 W and (b) from 0 to 500 W and from 500 to 1000 W. (Blue line) $P$ and (black line) $Q$.

Fig. 18 shows the synchronization process of the inverter with the grid. As shown, in less than 1 s, the inverter is synchronized to the grid. Then, the inverter can be connected to the grid, and at this moment, we can change the power references, as also shown in Fig. 18.

Fig. 19 shows the dynamics of the active power when changing the reference from 0 to 1 kW, from 0 to 500 W, and from 500 to 1000 W while keeping $Q = 0$ var. Fig. 20 shows the
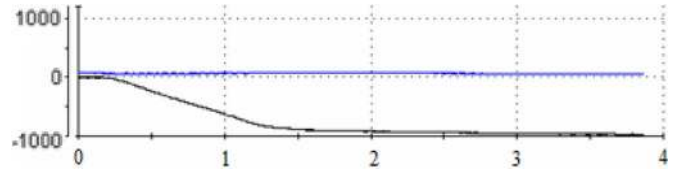


Fig. 20. Reactive power transient response from 0 to $-1000$ var for $P = 0$ W. (Blue line) $P$ and (black line) $Q$.
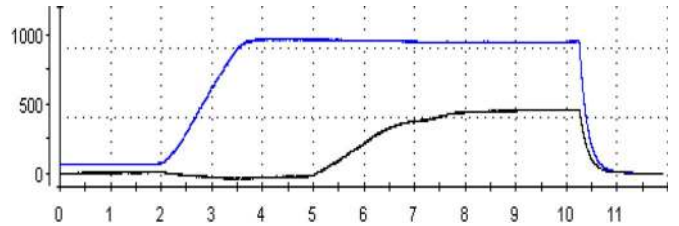


Fig. 21. Transition from islanding to grid-connected mode: (a) Synchronization process (grid and VSI voltages) and (b) $P$ and $Q$ for $t > 2$ s in islanding mode and $t > 2$ s in grid-connected mode. In $t = 5$ s, $P$ changes from 0 to 1000 W, in $t = 10$ s, $Q$ changes from 0 to 500 var, and in $t = 11$ s, the system is disconnected. (Blue line) $P$ and (black line) $Q$.

capability of the VSI to absorb 1000 var of reactive power. Notice the transient response and steady-state performances that endow the controller to the system.

Fig. 21 shows the transition from islanded to grid-connected mode. Then, the active and reactive power injected to the grid can be independently controlled. Finally, the system is intentionally disconnected. Notice the good agreement between the experimental results and the corresponding simulation results shown in Fig. 15(b).

Fig. 17 shows the supervisor panel with all the proposed control strategy. It is composed of its inner (voltage and current control) and outer loops (synchronization and power sharing). Some system measurements can be appreciated as well in order to analyze the system behavior within specified limits.

## VII. CONCLUSION

This paper has presented a novel control for a VSI that is able to operate in islanding mode, as well as in grid-connected mode. In this last case, the inverter is able to inject the desired active and reactive power to the grid. The control has two main structures. The first one is the grid parameter estimation, which calculates the amplitude and frequency of the grid, as well as the magnitude and phase of the grid impedance. The second one is a droop-control scheme, which uses these parameters to inject independently active and reactive power to the grid. The proposed droop control uses such parameters to close the loop, achieving a tight $P$ and $Q$ regulation. Owing to the feedback variables of the estimator, the system dynamics is well decoupled from the grid parameters. The results point out the applicability of the proposed control scheme to DG VSIs for microgrid applications.

## REFERENCES

[1] P. L. Villeneuve, "Concerns generated by islanding," *IEEE Power Energy Mag.*, vol. 2, no. 3, pp. 49–53, May/Jun. 2004.
[2] T. Kawabata and S. Higashino, "Parallel operation of voltage source inverters," *IEEE Trans. Ind. Appl.*, vol. 24, no. 2, pp. 281–287, Mar./Apr. 1988.

[3] M. C. Chandorkar and D. M. Divan, "Control of parallel connected inverters in standalone AC supply system," *IEEE Trans. Ind. Appl.*, vol. 29, no. 1, pp. 136–143, Jan./Feb. 1993.

[4] S. Barsali, M. Ceraolo, P. Pelacchi, and D. Poli, "Control techniques of dispersed generators to improve the continuity of electricity supply," in *Proc. IEEE PES Winter Meeting*, 2002, pp. 789–794.

[5] D. M. Vilathgamuwa, P. C. Loh, and Y. Li, "Protection of microgrids during utility voltage sags," *IEEE Trans. Ind. Electron.*, vol. 53, no. 5, pp. 1427–1436, Oct. 2006.

[6] S. Chakraborty, M. D. Weiss, and M. G. Simoes, "Distributed intelligent energy management system for a single-phase high-frequency AC microgrid," *IEEE Trans. Ind. Electron.*, vol. 54, no. 1, pp. 97–109, Feb. 2007.

[7] R. Teodorescu and F. Blaabjerg, "Flexible control of small wind turbines with grid failure detection operating in stand-alone and grid-connected mode," *IEEE Trans. Power Electron.*, vol. 9, no. 5, pp. 1323–1332, Sep. 2004.

[8] J. M. Guerrero, J. Matas, L. García de Vicuña, M. Castilla, and J. Miret, "Decentralized control for parallel operation of distributed generation inverters using resistive output impedance," *IEEE Trans. Ind. Electron.*, vol. 54, no. 2, pp. 994–1004, Apr. 2007.

[9] M. Prodanovic and T. C. Green, "High-quality power generation through distributed control of a power park microgrid," *IEEE Trans. Ind. Electron.*, vol. 53, no. 5, pp. 1471–1482, Oct. 2006.

[10] X. Yuan, W. Merk, H. Stemmler, and J. Allmeling, "Stationary-frame generalized integrators for current control of active power filters with zero steady-state error for current harmonics of concern under unbalanced and distorted operating conditions," *IEEE Trans. Ind. Appl.*, vol. 38, no. 2, pp. 523–532, Mar./Apr. 2002.

[11] J. C. Vasquez, J. M. Guerrero, E. Gregorio, P. Rodríguez, R. Teodorescu, and F. Blaabjerg, "Adaptive droop control applied to distributed generation inverters connected to the grid," in *Proc. IEEE ISIE*, 2008, pp. 2420–2425.

[12] P. Rodríguez, A. Luna, M. Ciobotaru, R. Teodorescu, and F. Blaabjerg, "Advanced grid synchronization system for power converters under unbalanced and distorted operating conditions," in *Proc. IEEE IECON*, 2006, pp. 5173–5178.

[13] A. de Oliveira, J. C. de Oliveira, J. W. Resende, and M. S. Miskulin, "Practical approaches for AC system harmonic impedance measurements," *IEEE Trans. Power Del.*, vol. 6, no. 4, pp. 1721–1726, Oct. 1991.

[14] L. Asiminoaei, R. Teodorescu, F. Blaabjerg, and U. Borup, "Implementation and test of an online embedded grid impedance estimation technique for PV inverters," *IEEE Trans. Ind. Electron.*, vol. 52, no. 4, pp. 1136–1144, Aug. 2005.

[15] F. Bertling and S. Soter, "A novel converter integrable impedance measuring method for islanding detection in grids with widespread use of decentral generation," in *Proc. Power Electron., Elect. Drives, Autom. Motion*, 2006, pp. 503–507.

[16] M. Sumner, B. Palethorpe, and D. W. P. Thomas, "Impedance measurement for improved power quality—Part 2: A new technique for standalone active shunt filter control," *IEEE Trans. Power Del.*, vol. 19, no. 3, pp. 1457–1463, Jul. 2004.

[17] J. Huang and K. A. Corzine, "AC impedance measurement by line-to-line injected current," in *Conf. Rec. IEEE IAS Annu. Meeting*, 2006, pp. 300–306.

[18] J. P. Rhode, A. W. Kelley, and M. E. Baran, "Complete characterization of utilization-voltage power system impedance using wideband measurement," *IEEE Trans. Ind. Appl.*, vol. 33, no. 6, pp. 1472–1479, Nov./Dec. 1997.

[19] A. R. Bergen, *Power Systems Analysis*. Englewood Cliffs, NJ: Prentice-Hall, 1986.

[20] J. M. Guerrero, J. Matas, L. García de Vicuña, M. Castilla, and J. Miret, "Wireless-control strategy for parallel operation of distributed-generation inverters," *IEEE Trans. Ind. Electron.*, vol. 53, no. 5, pp. 1461–1470, Oct. 2006.

[21] E. A. A. Coelho, P. Cabaleiro, and P. F. Donoso, "Small signal stability for single phase inverter connected to stiff AC system," in *Conf. Rec. IEEE IAS Annu. Meeting*, 1999, pp. 2180–2187.

[22] J. M. Guerrero, J. C. Vasquez, J. Matas, J. L. Sosa, and L. García de Vicuña, "Parallel operation of uninterruptible power supply systems in microgrids," in *Proc. EPE*, 2007, pp. 1–9.

[23] Y. Li, D. M. Vilathgamuwa, and P. C. Loh, "Design, analysis, and real-time testing of a controller for multibus microgrid system," *IEEE Trans. Power Electron.*, vol. 19, no. 5, pp. 1195–1204, Sep. 2004.

[24] P. Rodríguez, A. Luna, I. Candela, R. Teodorescu, and F. Blaabjerg, "Grid synchronization of power converters using multiple second order generalized integrators," in *Proc. IEEE IECON*, 2008, pp. 755–760.

[25] B. Zhang, D.-W. Wang, K.-L. Zhou, and Y.-G. Wang, "Linear phase lead compensation repetitive control of a CVCF PWM inverter," *IEEE Trans. Ind. Electron.*, vol. 55, no. 4, pp. 1595–1602, Apr. 2008.

[26] R.-J. Wai, W.-H. Wang, and C.-Y. Lin, "High-performance stand-alone photovoltaic generation system," *IEEE Trans. Ind. Electron.*, vol. 55, no. 1, pp. 240–250, Jan. 2008.

[27] H. Deng, R. Oruganti, and D. Srinivasan, "A simple control method for high-performance UPS inverters through output-impedance reduction," *IEEE Trans. Ind. Electron.*, vol. 55, no. 2, pp. 888–898, Feb. 2008.

[28] C.-M. Wang, C.-H. Su, M.-C. Jiang, and Y.-C. Lin, "A ZVS-PWM single-phase inverter using a simple ZVS-PWM commutation cell," *IEEE Trans. Ind. Electron.*, vol. 55, no. 2, pp. 758–766, Feb. 2008.

[29] L.-H. Li, T.-T. Jin, and K. M. Smedley, "A new analog controller for three-phase voltage generation inverter," *IEEE Trans. Ind. Electron.*, vol. 55, no. 8, pp. 2894–2902, Aug. 2008.

[30] H. Tao, J. L. Duarte, and M. A. M. Hendrix, "Line-interactive UPS using a fuel cell as the primary source," *IEEE Trans. Ind. Electron.*, vol. 55, no. 8, pp. 3012–3021, Aug. 2008.

[31] J. M. Guerrero, J. C. Vasquez, J. Matas, M. Castilla, and L. García de Vicuña, "Control strategy for flexible microgrid based on parallel line-interactive UPS systems," *IEEE Trans. Ind. Electron.*, vol. 56, no. 3, pp. 726–736, Mar. 2009.

**Juan C. Vasquez** received the B.S. degree in electronics engineering from the Universidad Autonoma de Manizales, Manizales, Colombia, in 2004. He is currently working toward the Ph.D. degree in the Department of Automatic Control Systems and Computer Engineering, Universitat Politecnica de Catalunya, Spain.

He has been an Assistant Professor teaching courses on digital circuits, servo systems, and flexible manufacturing systems at the Universidad Autonoma de Manizales. His research interests include modeling, simulation, and management applied to distributed generation in microgrids.

**Josep M. Guerrero** (S'01–M'04–SM'08) received the B.S. degree in telecommunications engineering, the M.S. degree in electronics engineering, and the Ph.D. degree in power electronics from the Universitat Politecnica de Catalunya, Barcelona, Spain, in 1997, 2000, and 2003, respectively.

He is an Associate Professor in the Department of Automatic Control Systems and Computer Engineering, Universitat Politecnica de Catalunya, where he currently teaches courses on digital signal processing, control theory, microprocessors, and renewable energy. Since 2004, he has been responsible for the Renewable Energy Laboratory, Escola Industrial de Barcelona, Barcelona, Spain. His research interests include photovoltaics, wind energy conversion, uninterruptible power supplies, storage energy systems, and microgrids.

Dr. Guerrero is an Associate Editor of the IEEE TRANSACTIONS ON INDUSTRIAL ELECTRONICS and the IEEE TRANSACTIONS ON POWER ELECTRONICS. He is the Editor-in-Chief of the *International Journal of Integrated Energy Systems*. He is also an Associate Editor of the *International Journal of Power Electronics* and the *International Journal of Industrial Electronics and Drives*.

**Alvaro Luna** received the B.S. and M.S. degrees in electrical engineering from the Universitat Politecnica de Catalunya (UPC), Terrassa, Spain, in 2001 and 2005, where he is currently working toward the Ph.D. degree.

In 2005, he joined the faculty of the Department of Electrical Engineering, UPC, as an Assistant Professor.

**Pedro Rodríguez** (S'99–M'04) received the B.S. degree in electrical engineering from the University of Granada, Granada, Spain, in 1989, and the M.S. and Ph.D. degrees in electrical engineering from the Universitat Politecnica de Catalunya (UPC), Barcelona, Spain, in 1994 and 2004, respectively.

In 1990, he joined the faculty of UPC as an Assistant Professor, where he is currently an Associate Professor in the Department of Electrical Engineering, the Head of the Research Group on Renewable Electrical Energy Systems, and the Cosupervisor of the Vestas Power Program in partnership collaboration with Aalborg University (AAU), Aalborg, Denmark. In 2005, he was a Visiting Researcher at the Center for Power Electronics Systems, Virginia Polytechnic Institute and State University, Blacksburg. In 2006 and 2007, he was a Postdoctoral Researcher at the Institute of Energy Technology, AAU, where he has been lecturing Ph.D. courses since 2006. He has coauthored about 100 papers in technical journals and conference proceedings. He is the holder of four patents. His research interest is focused on applying power electronics to distributed energy systems and power quality.

Dr. Rodriguez is a member of the IEEE Power Electronics Society, IEEE Industry Applications Society, IEEE Industrial Electronics Society (IES), and the IEEE IES Technical Committee on Renewable Energy Systems. He is an Associate Editor of the IEEE TRANSACTIONS ON POWER ELECTRONICS and the General Chair of the IEEE Industrial Electronics Student Forum.

**Remus Teodorescu** (S'94–A'97–M'99–SM'02) received the Dipl.Ing. degree in electrical engineering from the Polytechnical University of Bucharest, Bucharest, Romania, in 1989, and the Ph.D. degree in power electronics from the University of Galati, Galati, Romania, in 1994.

In 1998, he joined the Power Electronics Section, Institute of Energy Technology, Aalborg University, Aalborg, Denmark, where he is currently a Full Professor, the Founder and Coordinator of the Green Power Laboratory, focusing on the development and testing of grid converters for renewable energy systems, and the Coordinator of the Vestas Power Program. He has published more than 120 papers, in addition to one book, and three patents (pending). His areas of interest are design and control of power converters used in renewable energy systems, distributed generation, mainly wind power and photovoltaics, computer simulations, and digital control implementation.

Dr. Teodorescu is an Associate Editor of the IEEE POWER ELECTRONICS LETTERS and the Chair of the IEEE Danish joint Industrial Electronics Society/Power Electronics Society/Industry Applications Society (IAS) chapter. He was a corecipient of Technical Committee Prize Paper Awards at the IEEE IAS Annual Meeting 1998 and the Third-ABB Prize Paper Award at IEEE Optim 2002.